Adv Polym Sci
DOI: 10.1007/12_2017_40

Influence of Topography on Adhesion and Bioadhesion

Donglee Shin and J.Carson Meredith

Abstract Nature, through evolution, has developed many different structured adhesive systems to create strong and reliable adhesion on various substrates, including those with rough or smooth surfaces under dry and wet conditions. However, the details of the adhesive interactions of structured or roughened surfaces are just beginning to be resolved. This chapter examines the physical principles of dry and wet adhesion of structured surfaces from simple to complex geometries. A particular emphasis is placed on bioadhesive systems that achieve an impressive level of control over adhesion via fascinating structural features such as fibrils and spines. The influence of surface morphology and roughness on adhesion is also covered. Recent studies show that the attachment abilities of bioadhesive systems are dramatically reduced below a critical roughness. Based on this and other principles borrowed from nature, strategies can be pursued to create anti-adhesive surfaces via manipulating the surface topography of the substrate.

Keywords Adhesion • Bioadhesion • Contact mechanics • Surface morphology • Surface topography

Contents

D. Shin and J.C. Meredith (✉)
School of Chemical & Biomolecular Engineering, Renewable Biomaterials Institute, Georgia Institute of Technology, Atlanta, GA, USA
e-mail: carson.meredith@chbe.gatech.edu

List of Abbreviations

A	Hamaker constant
a	Contact area
b	Slip length
C	Coefficient in the atom-atom pair potential
D	Separation distance
D_0	Cutoff separation distance
D_w	Separation distance (wet adhesion models)
d	Interplanar separation
F	External loading force
F_{DMT}	Pull-off force (DMT model)
F_{JKR}	Pull-off force (JKR model)
H_w	Meniscus height
h_l	Thickness of liquid film
K	Elastic modulus
k_1	Proportionality factor (Rabinovich's model)
l_a	Azimuthal radius
N	Total number of liquid bridges
p_1, p_2	Number of atoms in unit volume
$p(z)$	Peak height distribution function
R	Radius of sphere
R_c	Contact radius
R_{LS}	Radius of sphere (Rumpf's model, Rabinovich's model)
R_p	Mean peak radius
R_S	Radius of sphere (JKR model, DMT model)
R_w	Radius of sphere (wet adhesion models)
r	Radius of small hemispherical asperities (Rumpf's, Rabinovich's models)
r_m	Meridional radius
rms	Root-mean-square
W_{12}	Work of adhesion
x	Ratio between the contact radius and half of the cutoff separation distance
γ, γ_l	Surface tension
η	Viscosity of liquid
θ, θ_l	Contact angle
λ	Peak-to-peak distance
ϕ	Filling angle
Ω	Meniscus area
ΔP	Laplace pressure
f^*	Correction factor to account for the effect of a partial slip boundary

1 Introduction

This chapter introduces the fundamentals of adhesion relevant to other chapters by discussing the causes and prevention of accumulated insect residues and ice on aircraft and biofouling constituents on marine surfaces. Using natural and man-made examples, this contribution aims to review the effects of microscale and nanoscale topography on adhesion, caused by the potential role of topography in future solutions to the problems of residue accumulation. Nanostructured surfaces have been studied widely because of the fascinating functions they enable, such as anti-wetting [1], anti-icing [2], water droplet harvesting [3] and mobilization [4], photonic color [5], turbulent fluid drag reduction [6], and glueless adhesion [7]. Although man-made approaches for these functions exist, each of these functions is also naturally occurring. The surface structures of animals and plants have evolved in many instances to confer specific functionalities that improve survival or reproduction. For example, lotus leaves possess a superhydrophobic (water-repellent) surface attributed to a hierarchical structure containing both micrometer- and nanometer-scale features [8, 9] (Fig. 1a, b), and this function improves the efficiency of photosynthesis by facilitating self-cleaning mechanisms. The micropatterned structures of hydrophobic and hydrophilic regions on the back of desert beetles promote water condensation to collect water droplets from humid air [10] (Fig. 1c, d). Some butterflies use structural colors, created by controlling the transport of light via photonic nanostructures, to produce vivid and bright wing colors with low energy consumption [11] (Fig. 1e, f). The aligned riblet structures on shark skin reduce the drag experienced by fast-swimming sharks in turbulent flow [12] (Fig. 1g, h).

Many plants and animals have evolutionarily optimized surface structures that create strong and functional adhesion for locomotion or transportation. For example, the multi-branched structure of gecko foot hairs creates exceptionally strong adhesion to enable climbing on both smooth and rough surfaces without an adhesive secretion [13]. The hairy structures (200–500 nm long and 15 nm thick) on the gecko setae (30–130 μm long) allow the foot pads to create contact area sufficient to sustain the gecko's body weight, even on vertical walls. Tree frogs can adhere strongly to wet and rough surfaces. The adhesive pads of tree frogs have hexagonal cells (approximately 10 μm in diameter) separated by deep channels (1 μm wide) filled with a mucus secretion. The microstructured channels are the paths for distributing mucus over the whole contact area between the adhesive pad and a contact surface, and the channels also work to drain water, enabling attachment on water-coated surfaces [14]. Insects have both hairy and smooth adhesive pads whose adhesion is mediated by thin layers of adhesive secretions [15]. The tip radius of structures on the hairy adhesive pad are a size roughly ranging from 1 to 10 μm, and these can attach at multiple points to create a large contact area on a rough surface [15, 16], similar to the action of the gecko setae. The smooth adhesive pad, which is a "pillow-like" soft structure that consists of branching fibrils and the outer cuticle layer [17], can also adapt to surface roughness features to create large

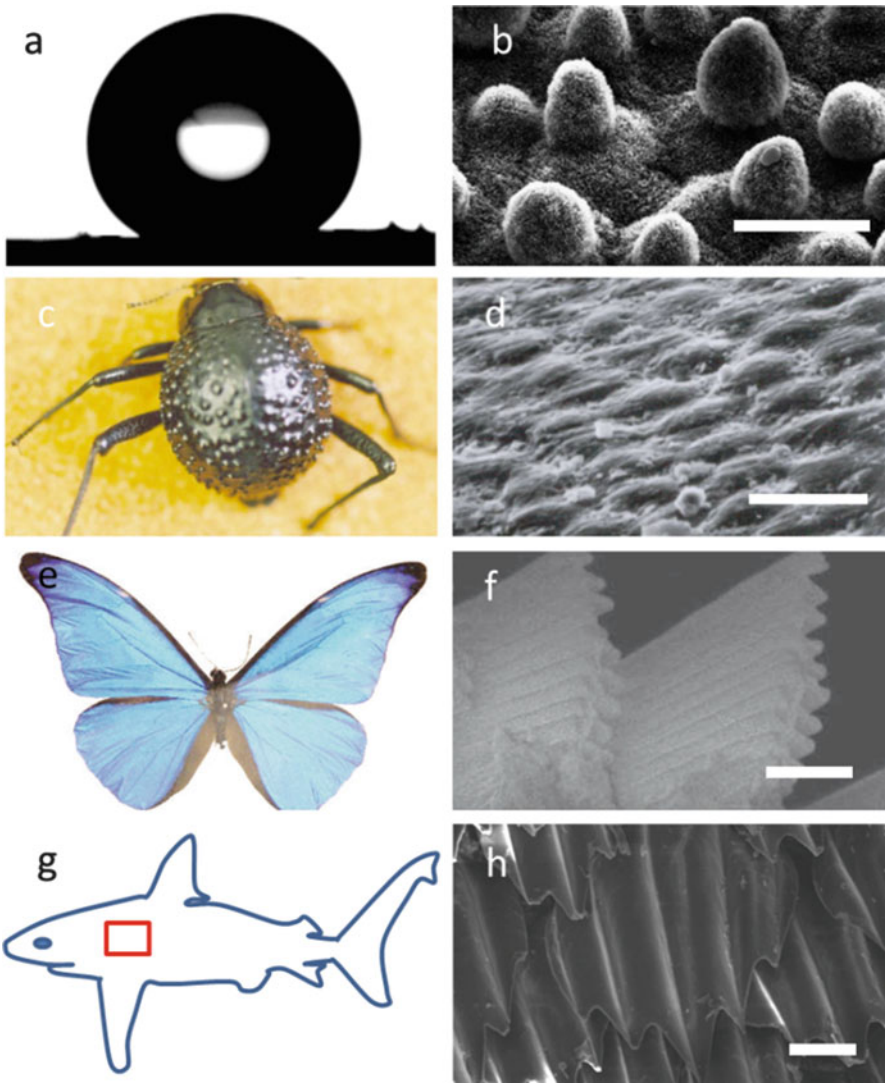

Fig. 1 (**a**) Water droplet on a lotus leaf CA = 152°. (Reproduced with permission from Hao et al. [8].) (**b**) Scanning electron microscopy (SEM) image of the lotus leaf. (Reproduced with permission from Barthlott et al. [9].) (**c**, **d**) Photograph and SEM image of the water-harvesting surface of the desert beetle. (Reproduced with permission from Parker et al. [10].) (**e**, **f**) Photograph and SEM image of distinctive iridescent blue color of the wings of *Morpho* butterfly. (Reproduced with permission from Parker et al. [11].) (**g**, **h**) Cartoon and SEM image of the scale structure of shark skin. (Reproduced with permission from Luo et al. [12].) *Scale bars* = 20 μm (**b**), 10 μm (**d**), 400 nm (**f**), and 50 μm (**h**)

contact areas for strong adhesion. Pollens from different plant species display a remarkable variety of ornamentations with unique size, shape, and density on their exine (shell) surface. When pollens interact with a structured flower stigma, their surface features cause pressure-sensitive adhesion mediated by mechanical interlocking [18]. Pollen grains exhibiting structural ornamentations have been shown to adhere strongly to the stigma surfaces within the same botanical family [19], which is thought to facilitate reproduction.

In addition to these examples of natural adhesive structures, examples exist in nature of anti-adhesive and slippery surfaces as well. A prominent example is the pitcher plant *Nepenthes alata*, which possesses both anti-adhesive cuticular wax surfaces [20] and a slippery peristome consisting of grooved structures that are continuously wetted by water in humid environments [21]. Whereas the waxy cuticle reduces normal adhesion forces of insects such as ants, the wetted peristome presents a lubricated low-shear interface, on which insects slide into the pitcher where they are digested. The lubricant infusion of *Nepenthes* has inspired the engineering of synthetic lubricant–infused surfaces that promote sliding and resist attachment of particles, ice, and other contaminants [22, 23]. Another example of anti-adhesive structures is the riblets of shark skin (Fig. 1h), which have been mimicked by surface wrinkling to produce biofouling resistance [24].

Numerous researchers have studied the adhesion mechanisms of simple geometries, such as plane-plane, sphere-sphere, cone-cone, sphere-plane, sphere-cylinder, and cone-plane over the past several decades [25–31]. Based on this background knowledge, studies of the influence of geometry on adhesion have more recently expanded to treat surfaces with complex fine features. The investigation of bioadhesion, such as in the examples mentioned above, has been an important part of an emerging understanding of the effects of microscale and nanoscale topography on adhesion. Herein, we discuss the basic physical principles of adhesion with simple geometric models as the adhesion of complex structured surfaces is also based on the same physical principles. These include van der Waals (vdW), capillary, and viscous forces (Sect. 2). Then we discuss how different surface geometries (hairy, smooth, and echinate) affect adhesive mechanisms and focus on the dependence of bioadhesion on substrate structure (Sect. 3). We also review recent efforts to produce anti-adhesive surfaces based on surface topography designed from natural adhesive phenomena (Sect. 4). Because of the primary importance of wet adhesion – adhesion between solids that is mediated by liquids – in the problems of aircraft and marine surface bioadhesion, this review focuses in particular on the static and dynamic contributions of capillary forces to adhesion. As a result, we do not consider in detail the contributions of dynamics in deformable bodies on solid adhesion, such as the role of shear forces in soft solid–solid adhesion. However, these are significant in many soft biological adhesion systems, and there are excellent recent reviews available on this topic [32–34]. By examining adhesion fundamentals as well as examples taken from natural systems, we hope to motivate thoughts about how aircraft or marine surface features could be designed to prevent or mitigate adhesion of contaminants (Fig. 2).

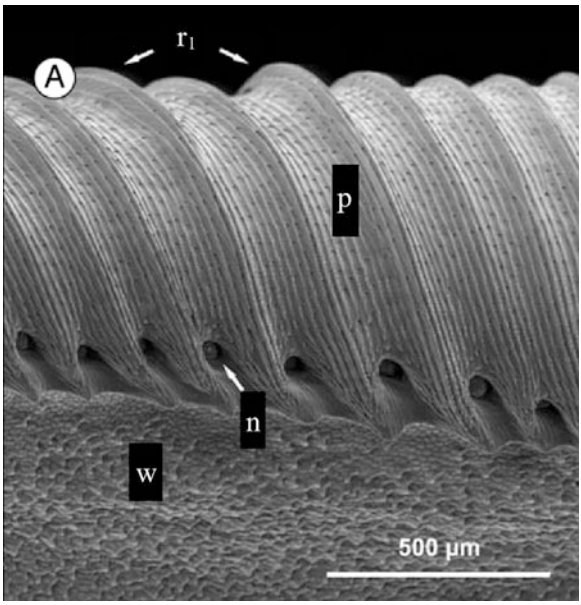

Fig. 2 SEM image of pitcher plant *N. alata* peristome surface (p), showing the first- (r_1) and second-order radial ridges, extrafloral nectaries (n), and waxy inner wall surface (w). Reproduced with permission from Bauer et al. [21]

2 Physical Principles of Adhesion

A practical question that this volume seeks to address is how aircraft and marine surfaces can be designed to minimize adhesion in extreme environments. It is important to begin by defining the concepts. Adhesion refers to the energy or work required to separate two surfaces that are already in contact. Although events that occur during the impact of insects with aircraft are important in determining the contact area, and are discussed in detail elsewhere in this volume [35], we consider adhesion here to be the resistance to surface separation after contact is established. A separate, but related topic is that of surface friction, which displays itself in perceived properties of surface slipperiness. Slippery surfaces often also exhibit low adhesion, but strictly speaking they are not always correlated. Friction relates to the lateral forces occurring when contacting surfaces are moved parallel to one another (shearing), whereas adhesion relates to the movement of surfaces away (normal direction) from one another. The fascinating behavior of slippery surfaces in nature has been the subject of recent work, such as the lubricated surfaces of the pitcher plant [23, 36], and this behavior can undermine initial adhesive contact by promoting sliding.

Animals and plants utilize transitory (nonpermanent) adhesive force for transport and locomotion [37, 38], and this temporary adhesion is strongly affected by the topography of the adhesive surface. Adhesive mechanisms related to transitory bioadhesion can be classified roughly into two categories: (1) dry adhesion based on intermolecular forces and (2) wet adhesion based on liquid-mediated static and

dynamic capillary forces. These mechanisms are also operative in synthetic adhesives in manmade materials, such as pressure-sensitive adhesives [39], latex paints [40], ink toner, and powder coatings [41]. In this section we discuss the physical principles of both dry and wet adhesive mechanisms with representative simple geometry models.

These adhesion fundamentals relate to the problem of biological residue accumulation in extreme environments in a number of ways. After insect impact on aircraft, the adhesion of hemolymph is expected to be governed initially by a combination of capillary static and dynamic forces that resist removal from the surface. As hemolymph gels and solidifies, adhesion becomes dominated by dry adhesive forces that are likely controlled by vdW and specific noncovalent interactions with the aircraft surfaces. Adhesion of other solid contaminants on aircraft (including ice) surfaces varies between these dry and wet mechanisms depending on the presence of a wetting fluid that may form capillary bridges between the solid surfaces. Of course, it is expected that adhesion of biological fluids or solids, including those of living animals such as diatoms, mussels, or barnacles, on marine underwater surfaces may involve vdW forces, specific interactions, covalent bonding, and capillarity, as well as mechanical contributions from shearing and viscoelasticity.

In general, the adhesive force of neutral surfaces in a 'dry' atmosphere, such as nitrogen or vacuum, is comprised of vdW interactions, and hydrogen, covalent, or metallic bonds [42]. The energy of vdW interactions is normally much smaller than covalent or hydrogen bonds. However, the vdW interaction plays a prominent role in determining the attractive force magnitude of surfaces and colloids because the vdW interaction has a longer range (0.2–10 nm) than the other inter- or intramolecular bonding (covalent, hydrogen, and metallic bonding) scales (normally 0.1–0.2 nm) [43]. Even though there is no universal model that accounts for the influence of all contributions (e.g., elastic moduli, surface energy, temperature, relative humidity, and Hamaker constant) on vdW interactions, the following adhesion models for simple geometry help us to understand the physical principles of dry adhesion. Common classical models to estimate the adhesion force between two elastic spheres (or sphere and planar surfaces) originated from Hertzian theory [44]. In 1882 Heinrich Hertz developed a model for the contact area (a) of two elastic spheres (of radii R_1 and R_2 with elastic moduli K) with external loading force (F) [43]:

$$a = \left(\frac{FR}{K}\right)^{1/3}, \tag{1}$$

where $R = R_1R_2/(R_1 + R_2)$.

In Hertzian theory, the intermolecular attraction between contact surfaces was ignored, so the contact area is apparently zero when there is no (or negative) external load. In 1971, Johnson, Kendall, and Roberts (JKR) developed a theory to estimate the adhesion between two solid surfaces [45]. They observed that the experimentally measured contact areas were larger than values estimated by Hertz

theory, and they confirmed that the solid surfaces still adhered under zero or small negative external loading force. They proposed that the surface interaction affects both deformed shape and overall loading force, which is represented by the sum of the external loading force and adhesion of the surfaces. The deformed contact area was derived as follows [46]:

$$a^3 = \frac{R}{K}\left(F + 3\pi W_{12}R + \left(6\pi W_{12}RF + (3\pi W_{12}R)^2\right)^{1/2}\right), \tag{2}$$

where F is external load and W_{12} is work of adhesion, which is the work done in separating a unit area of the interface. For a sphere (radius of sphere, $R_s = R_1$) on a flat surface ($R_2 = \infty$), the adhesion or pull-off force can be derived as [47]

$$F_{\mathrm{JKR}} = \frac{3}{2}\pi R_s W_{12}. \tag{3}$$

Unlike the JKR case, Derjaguin, Muller, and Toporov (DMT) assumed that the shape of the contacting surfaces is not affected by surface intermolecular interactions [48]. Therefore, the deformed contact area could be derived as [46]

$$a^3 = \frac{R}{K}(F + 2\pi W_{12}R), \tag{4}$$

and adhesion or pull-off force of a sphere on a flat surface can be derived as [47]

$$F_{\mathrm{DMT}} = 2\pi R_s W_{12}. \tag{5}$$

The JKR and DMT models consider the deformation of the contact area, but neither model accounts for the influence of separation distance on adhesion. When the contact surfaces have roughness or geometrical features, the assumption of complete contact is no longer valid and the separation distance of the surfaces must be considered [49]. The separation distance is the most significant factor defining adhesive force magnitude in the nonretarded region (separation distance less than 5 nm) [43]. Therefore, the adhesion models for rough or structured surfaces often use the Hamaker approach as a starting point. Hamaker proposed that the adhesion between particles and surfaces can be estimated by the integration of the vdW pair potential between all atoms in one body and all atoms in the other body [25]. In his study, the vdW interaction between a sphere and a flat surface was derived as

$$F_{\mathrm{vdw}} = -\frac{A_{132}}{24R_c}\left(\frac{2}{x} - \frac{1}{x^2} - \frac{2}{x+1} - \frac{1}{(x+1)^2}\right), \tag{6}$$

where A_{132} is the material-dependent nonretarded Hamaker constant, which represents the magnitude of interaction of the two interacting bodies (1 and 2) consisting of atoms with induced dipoles across a medium (3). The Hamaker constant can be determined by [43]

$$A = \pi^2 C p_1 p_2, \tag{7}$$

where p_1 and p_2 are the number of atoms in a unit volume of the two bodies (1 and 2), and C is the coefficient in the atom-atom pair potential. The x in (6) represents the ratio between the contact radius (R_c) and half of the cutoff separation distance (D_0), which is the predicted separation distance of contacting surfaces. (Some references approximate the cutoff distance at around 0.3–0.4 nm [49, 50], but others evaluate it as 0.165 nm [13, 43].) Equation (6) can be simplified to (8) in the limit of $x << 1$ [43]:

$$F_{\text{vdw}} = \frac{A_{132} R_c}{6D^2}, \tag{8}$$

where D is separation distance.

It is well-known that the surface pattern and roughness reduce the adhesion between surfaces or a spherical particle and a planar surface [51, 52]. Rumpf's model is a common and simple model based on Hamaker's approach to consider the effect of nanoscale surface roughness on adhesion [53]. This model estimates the adhesion between a large spherical particle (radius R_{LS}) and a flat surface covered with small hemispherical asperities (radius r), and normal alignment of the center of the particle and asperity is assumed (Fig. 3a). Rumpf's model consists of two terms as shown in the following formula [53]:

$$F_{\text{Rumpf}} = \frac{A_{132}}{6D_0^2}\left[\frac{rR_{\text{LS}}}{r + R_{\text{LS}}} + \frac{R_{\text{LS}}}{\left(1 + \frac{r}{D_0}\right)^2}\right], \tag{9}$$

where D_0 is the cutoff distance. The first term represents the adhesion between the particle and hemispherical asperity in contact. The second term represents the "noncontact" attractive interaction between the particle and flat surface where

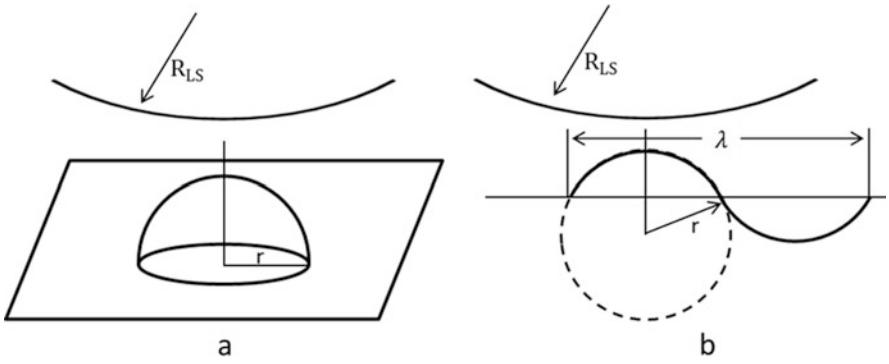

Fig. 3 Schematic illustration of the geometry proposed by: (**a**) Rumpf et al. [53]; (**b**) Rabinovich et al. [50]

separation distance is the radius of the hemispherical asperities. Rabinovich et al. found that Rumpf's model is not accurate in real systems with low roughness surface as it requires the center of a small hemisphere to be at the surface as shown in Fig. 3a [50]. In many real systems the center is located below the surface, and multiple surface asperities have contact with the large spherical particle. They proposed the approximation of this case with root-mean-square (rms) roughness and peak-to-peak distance (λ) (Fig. 3b) as shown in the following [50]:

$$F_{\text{Rabin.}} = \frac{A_{132}R_{\text{LS}}}{6D_0^2}\left[\frac{1}{1+\left(\frac{32R_{\text{LS}}k_1\text{rms}}{\lambda^2}\right)}+\frac{1}{\left(1+\frac{k_1\text{rms}}{D_0}\right)^2}\right], \tag{10}$$

where k_1 is a proportionality factor determined to be 1.817. In conventional adhesion and bioadhesion, surfaces can display surface roughness with a wide variety of structures and shapes, but the previous dry adhesion models are limited because of assumptions made about the shape or distribution of asperities. Recent dry adhesion models represent attempts to account for the interaction of complex contact shapes [16, 54], asymmetric structures [55], multiple contacts [56], and mechanical interlocking [57].

2.1 Wet Adhesion

In practical industrial and natural applications, wet adhesion is common. Strong wet adhesion driven by water condensation or by the presence of thin liquid lubricant on the contact surfaces is a critical issue in operation of fine-scale devices, including atomic force microscopy, magnetic storage devices, and fuel injectors [58]. For locomotion of animals, liquid secretions can create a larger contact area on a rough surface, compared to a dry surface because of strong capillary forces [59]. The mediating liquid can increase contact between the adhesive pad and a rough surface by filling the gaps between the pad and the surface. This is a topic of relevance to surface contamination in aerospace and marine applications, including biofouling, insect residue adhesion during hemolymph curing, and in-flight icing. The wet adhesion force can be split into two main components, capillary (meniscus) and viscous forces [60], as shown in (11):

$$F_{\text{Wet adhesion}} = F_{\text{Capillary force}} + F_{\text{Viscous force}}. \tag{11}$$

The vdW interaction may dominate wet adhesion in the case of very thin films (less than 10 nm), but its contribution is in most cases smaller than the capillary or viscous force. These forces are likely to be important in insect residues adhesion post-impact, that is, to prevent the residues from being driven off the surface by drag forces. The contribution of these primary components to wet adhesion can be

determined by considering the meniscus curvatures, dynamics, and viscosity of liquid films [58].

The capillary force is caused by a liquid meniscus (bridge) between two separated surfaces, and the curvature of the liquid meniscus is characterized by two radii, the azimuthal radius (l_a) and the meridional radius (r_m), shown in Fig. 4. The total capillary force between a sphere (radius, R_w) and a flat surface is defined as the summation of the surface tension and Laplace pressure contributions as shown in the following equation for a symmetric contact angle [58, 61]:

$$F_{\text{Capillary force}} = \Delta P \Omega + 2\pi R_w \gamma \sin\phi \sin(\phi + \theta), \tag{12}$$

where Ω is the meniscus area, ϕ is the filling angle, θ is the contact angle, γ is the surface tension of the liquid, and ΔP is Laplace pressure, estimated by the Young–Laplace equation:

$$\Delta P = \gamma \left(\frac{1}{l_a} - \frac{1}{r_m} \right). \tag{13}$$

The Young–Laplace equation describes the capillary pressure difference between two static phases. The surface tension and Laplace pressure forces explain the static contribution of the capillary liquid bridges to wet adhesion, but neither expression has dynamic terms. The contribution of hydrodynamic response can be estimated by a viscous force model, often called "Stefan adhesion" [60]. The viscous term of wet adhesion is a significant component of the wet adhesion mediated by highly viscous liquid capillary bridges, but it can also dominate for liquids of modest viscosity at high shear rate [62]. The viscous force acting on a sphere and a flat surface connected by a capillary bridge (Fig. 4) can be approximated by (14) [58]:

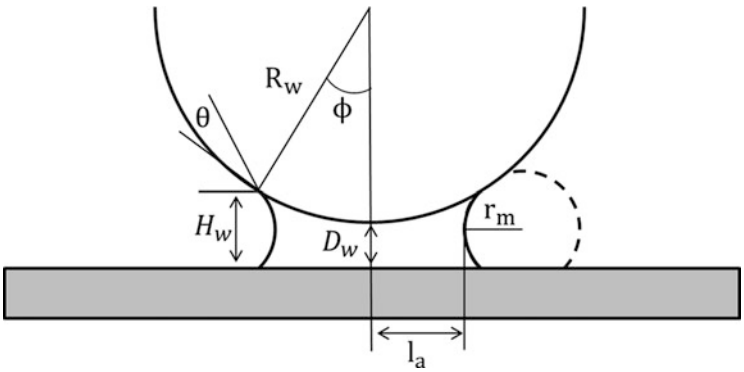

Fig. 4 Schematic of a meniscus bridge present at the interface between a sphere and a plane surface

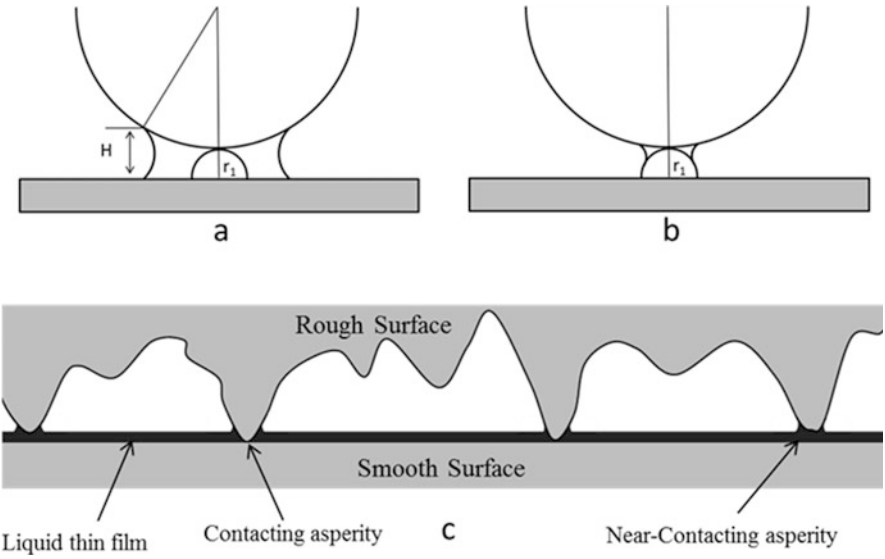

Fig. 5 Schematic of a liquid meniscus when: (**a**) $H > r_1$; (**b**) $H < r_1$. (**c**) Schematic for a rough surface in contact with a flat surface coated by a thin liquid film

$$F_{\text{Viscous force}} = 6\pi\eta R_w^2 \left[1 - \frac{D_w}{H_w}\right]^2 \frac{1}{D_w} \frac{\mathrm{d}D_w}{\mathrm{d}t}, \tag{14}$$

where η is the viscosity, D_w is the distance between a sphere and a flat surface, R_w is the radius of the spheres, H_w is the meniscus height, and $\mathrm{d}D_w/\mathrm{d}t$ is the separation rate. The total wet adhesion between a sphere and a flat surface can be estimated by the summation of (12) and (14).

The previous capillary (12) and viscous (14) force models are commonly used to estimate wet adhesion of a sphere and planar surface for simplicity, but the models fail to estimate accurately the wet adhesion for rough and patterned surfaces [63]. The topographical effect on capillary force is strongly dependent on the height of the liquid meniscus (the thickness of liquid) as shown in Fig. 5. When the meniscus height is greater than the hemispherical asperity as shown in Fig. 5a ($H > r_1$), the contact line and the curvatures of the meniscus are determined by the larger separation distance H. The previous (12) (sphere and flat surface model) is still valid as long as the increased separation distance is accounted for. However, when meniscus height is smaller than the hemispherical asperity (Fig. 5b), the wet adhesion model between two spheres (a large sphere and a small hemisphere) should be considered. The capillary force for interaction between two spheres was studied by Willett et al. [64] and Rabinovich et al. [65]. For multiple asperity contacts, Bhushan proposed a capillary force model of a randomly rough surface in contact with a smooth surface with a continuous liquid film as shown in Fig. 5c [66]. Both contacting and near-contacting asperities have a liquid meniscus, peak

radii (of the asperities) are assumed constant, and peak heights are assumed to follow a Gaussian distribution. By the summation of the wet adhesion on the asperities, the total wet adhesion of the surface is given as

$$F_{\text{Capillary force}} = 2\pi R_p \gamma_l (1 + \cos\theta_l) N \int_{d-h_l}^{\infty} p(z)\mathrm{d}z, \tag{15}$$

where N is the total number of liquid bridges, R_p is the mean peak radius, γ_l is the liquid surface tension, θ_l is the contact angle of the liquid in contact with the rough surface, d is the interplanar separation [62], h_l is the thickness of liquid film, and $p(z)$ is the peak height distribution function.

The viscous force acting between a sphere and a flat surface is generated by hydrodynamic drainage of liquid in the gap separating the surfaces. The surface topography affects the viscous force magnitude by creating slip or partial slip boundary conditions [67]. Remarkable hydrodynamic force reduction has been observed in capillaries on nanostructured surfaces [68, 69], such as structured superhydrophobic surfaces. The reduction is commonly explained by the slip boundary of liquid on trapped air pockets [70]. The classical viscous model (14) originates from Reynolds' lubrication theory with nonslip boundary conditions. Vinogradova initially proposed using a multiplying factor (f^*) to correct for the effect of a partial slip boundary, assuming creeping flow and the same slip length b for both surfaces [71]:

$$f^* = \frac{D_w}{3b}\left[\left(1 + \frac{D_w}{3b}\right)\ln\left(1 + \frac{6b}{D_w}\right) - 1\right]. \tag{16}$$

In practice, it is still challenging to estimate precisely the effective slip length because it is dependent on multiple factors, such as wettability, surface structure, and rheological properties of the liquid. However, recent studies have made meaningful progress in understanding the influence of diverse surface structures on boundary conditions of the viscous force model [72, 73].

3 Influence of Surface Geometry on Bioadhesion

The evolutionarily-adapted surfaces of animals and plants show how nature utilizes structure for functional adhesion. For example, the adhesive pads of animals support body weight on varying surfaces, such as smooth or rough, hydrophilic or hydrophobic, and clean or contaminated [74]. The structured adhesive pads and/or secretions both function critically to create strong but reversible adhesion for locomotion [38]. Plants also use structural surfaces and bioadhesives. For example, pollen grains use complex surface asperities and an adhesive liquid coating to facilitate transfer from anthers to pollinators, and from pollinators to stigmas [18, 75, 76]. In this section we discuss adhesive functional morphology in nature,

focusing on geckos, insects, tree frogs, and pollens. We also introduce experimental studies of the influence of structure on dry and wet adhesion, including the complex interactions of structure with surface roughness. It is hoped that lessons based on the evolved designs of nature can be applied to the prevention of adhesion in the extreme environments of aerospace and marine surfaces.

3.1 Functional Morphology of Bioadhesive Surfaces

3.1.1 Fibrillar Structure

It has been suggested that the adhesion of fibrillar structures on rough surfaces can be stronger than smooth surfaces [47] because fibrils with small effective elastic modulus can adapt to rough surfaces to increase contact area. Fine-scale hairs, with tip size less than the opposing surface roughness, can adapt to surface features, producing low strains on the hairs, increasing the fibrils total contact area [77]. In addition, it is well-known that the detachment of multifibrillar contacts requires more work than required to hold continuous contact [78], because the stored energy in a peeling fibril is not available for the detachment of the next fibril [47]. Therefore, many animals, from tiny mites to geckos and some mammals, take advantage of fibrillar adhesive pads to achieve strong adhesion on both smooth and rough surfaces.

In nature, the bioadhesive mechanism of hairy surfaces can be classified as dry or wet adhesion. Using a scaling analysis from mites to geckos, Gorb discussed the dependence of contact density on body mass [38]. He suggested that heavier animals, such as geckos and spiders, rely more on dry adhesion, and these animals tend to have compactly packed small fibrillar ends to create large peeling lines for strong adhesion [79]. However, recent studies claim that the total pad area of fibrillar systems is a main contributor to strong dry adhesion, not the high density of the fibrillar ends [80, 81].

Autumn et al. claimed that molecular vdW interactions are the dominant attractive force for gecko adhesion, as gecko adhesion was not affected by the hydrophobicity of the surface [13, 82]. Most gecko feet have hierarchical fibrillar structures consisting of lamellae, setae, branches, and spatulae [83], as shown in Fig. 6a–c. The second level of the hierarchy, consisting of the fibrillar 'setae' (ST in Fig. 6b), is typically 30–130 μm long and 5–10 μm in diameter, and the density is about 14,000 setae/mm^2. In many species these setae are split into multiple branches (BR in Fig. 6b, c) which are 20–30 μm long and 1–2 μm wide. Most setae terminate into 100–1,000 spatulae (SP in Fig. 6c) with a diameter of 0.1–0.2 μm [83]. To create strong adhesion, the fibrillar structures should be mechanically soft to achieve a large number of contacting hairs with low strains. However, if the hairs are too soft, they are intricately entangled, and adhesion is reduced significantly. The hierarchical structure is a solution to this problem. Hierarchical structures, such as lamellae and setae, provide the mechanical stability

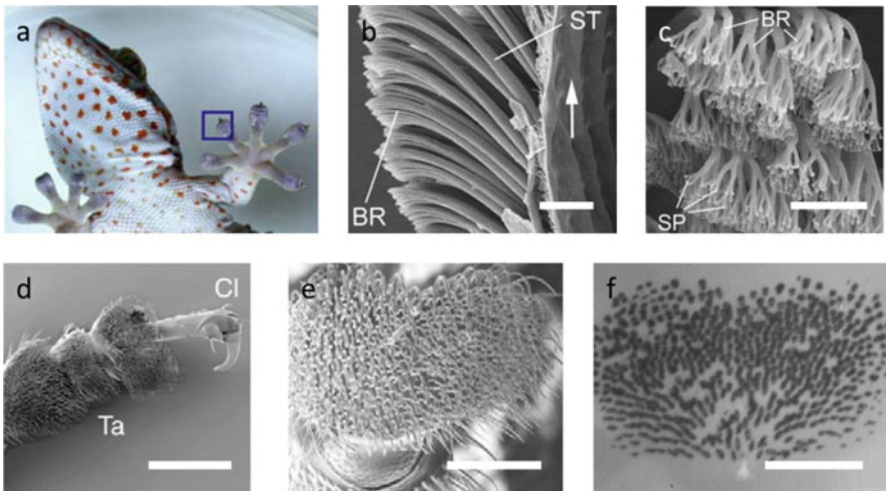

Fig. 6 (**a**–**c**) The hierarchical structure of *Gekko* gecko adhesive pads: (**a**) photograph of gecko toe; (**b**, **c**) scanning electron microscopy (SEM) images of branch (BR), seta (ST), and spatula (SP) in the adhesive pad of geckos. (Reproduced with permission from Gao et al. [84].) (**d**–**f**) The adhesive pad structure of a male dock beetle (*G. viridula*): (**d**, **e**) SEM images of the adhesive pad (Cl, claws; Ta, tarsal segments); (**f**) visualized contact area of the beetle adhesive pad with glass via epi-illumination. (Reproduced with permission from Bullock et al. [85].) *Scale bars* = 20 μm (**b**), 5 μm (**c**), 250 μm (**d**), 100 μm (**e**), and 100 μm (**f**)

attributed to relatively high modulus and thick diameter structures, whereas lower level hierarchy, such as branches and spatulae, provide compliance and adaptability to roughness [38, 86]. Another significant feature of gecko adhesion is the asymmetrical structure (slope) of the setae. When setae are attached on a surface, they are not vertical but tilted with respect to the surface, and that is the reason why the pull-off force of a single seta is strongly dependent on orientation [13]. It was observed that adhesion of a single seta was enhanced by more than an order of magnitude when the pulling angle was reduced from 90° to 30° [38, 87]. This result indicates that the asymmetrical structure of the setae plays a significant role in achieving reversible adhesion, which can be easily switched between attachment and detachment for locomotion.

Insects with fibrillar adhesive pads, such as reduviid bugs, flies, and beetles, utilize liquid adhesive secretions to increase attachment force [59]. Unlike geckos, the insects don't have complex hierarchical structures, and the setae of most insects end in a single and relatively large spatula (the areas of terminal contact of beetles and flies are larger than 1 μm^2) as shown in Fig. 6d–f. To increase the contact area of the large spatulae on a rough surface, insects fill the gap between the spatula and surface with a liquid adhesive secretion. It was observed that the adhesion of insect pads was reduced significantly by organic solvent washing [88], and insufficient adhesive forces were recorded when beetles were tested on a liquid-absorbing nanoporous substrate [89]. Those studies show that the force magnitude of overall

adhesion relies strongly on the capillary adhesion of the liquid bridges. In addition, the fibrillar structure allows multiple liquid bridges, which can produce a stronger total capillary force than a single liquid bridge with equal total liquid volume [90].

The contact geometries strongly affect the adhesive functions of the fibrillar adhesive pad [16, 91]. Mushroom- and spatula-shaped elements are commonly observed contact geometries in nature and are strongly related to the duration of adhesion [92]. Spatula-shaped elements require a shear force to generate adhesion, and these terminal elements are useful for short-term dynamic adhesion during fast locomotion because the contact can be easily detached by peeling within a few milliseconds. By contrast, the mushroom-shaped terminal elements are more suitable for creating long-term adhesion. These elements do not require external applied shear forces, and a relatively higher pull-off force is required to rupture the contact.

3.1.2 Smooth Structure

Smooth adhesive pads are observed from diverse animals such as ants, bees, stick insects, grasshoppers, tree frogs, and arboreal possums [93]. As mentioned before, unlike fibrillary adhesive systems, continuous surfaces cannot make a large number of contacts that adapt to the geometry of a rough surface. Thus, animals with smooth adhesive pads have developed strategies to overcome this limitation. One adaptation is the soft mechanical properties of the smooth adhesive pads, which have high deformability to adapt a larger contact area on rough surfaces. For example, the reported effective elastic modulus of the adhesive pad of tree frogs is in the range of 4–25 kPa [94], and it is one of the softest biological structures. Smooth pads have an ultrastructure consisting of cuticular rods (insects) [17] or hexagonal epithelial cells (tree frogs) [14], and the fine structures of the pads allow close contact with low strain on rough surfaces. All known smooth adhesive pads utilize thin liquid films, such as watery mucus of tree frogs, multi-phase adhesive secretion of insects, and sweat of arboreal possums, to fill the gap between the pads and substrates, and this liquid film helps to create a large contact area on rough surfaces.

Tree frogs are well-known heavy body mass amphibians that utilize smooth adhesive pads. The details of the adhesive mechanism still remain elusive, but it was found that the physical properties and surface structures of the smooth adhesive pad have a critical role in attachment on vertical and overhanging surfaces [95]. These adhesive pads (Fig. 7a) consist of regular hexagonal epithelial cells (10–15 μm) (Fig. 7b) separated by watery mucus-filled channels (1 μm wide). Each cell consists of densely-packed nanopillars (Fig. 7c) that are 300–400 nm in diameter with a concave end [96]. The thin intervening watery mucus layer between the pad and surface forms an essential part of wet adhesion. The capillary force generated by a liquid bridge around the edge of the pad, and the viscous force generated over the whole contact area, strongly contribute to the adhesion of tree frogs [96]. The channel structure on the pad surface works to distribute fluid across

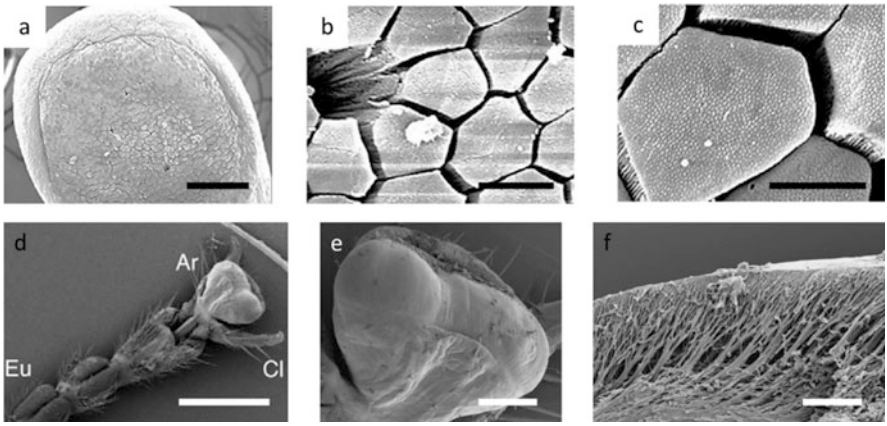

Fig. 7 (**a**–**c**) Scanning electron microscopy (SEM) images of tree fog (*Litoria caerulea*) adhesive pad: (**a**) toe pad; (**b**) hexagonal epithelial cell; (**c**) densely packed nanopillars. (Reproduced with permission from Scholz et al. [96].) (**d**–**f**) SEM images of Indian stick insect (*C. morosus*) adhesive pad: (**d**) front view of tarsal segments (Cl, claws; Eu, euplantulae; Ar, arolium); (**e**) the distal adhesive pad (reproduced with permission from Bullock et al. [85]); (**f**) cross-section view of the distal adhesive pad within the smooth cuticle layer (branching fibrils oriented almost perpendicular to the contact surface) (reproduced with permission from Dirks et al. [17]). *Scale bars* = 100 μm (**a**), 10 μm (**b**), 5 μm (**c**), 1,000 μm (**d**), 200 μm (**e**), and 20 μm (**f**)

the pad, similar to, for example, a tire tread, which allows for rapid drainage of liquid. The structured adhesive pad maintains an extremely thin liquid film for strong wet adhesion in air, and allows for the close contact of the pad with the surface under wet conditions [14]. Recently, the smooth pad morphology of torrent frogs, which are able to climb a vertical surface covered by flowing water, have been under investigation [97, 98]. It is proposed that the straight channels between elongated cells can accelerate drainage rate of excess fluid underneath the pad.

Many insects with smooth adhesive pads also utilize wet adhesion of the adhesive secretion as do the insects with fibrillar pads. The smooth pads (Fig. 7d) of the insects are a "pillow-like" soft structure (Fig. 7e) that consist of branching fibrils (Fig. 7f) oriented perpendicular to the surface within an outer cuticle layer [17]. This internal fibrous structure helps to increase adaptability to surface roughness, and it can be used to facilitate manipulation of the pad contact area via proximal pulling by the insects. It is not well-understood how the presence of a continuous liquid film between a smooth pad and substrate can create strong static attachment ability on a vertical surface. Dirks et al. suggested that the two-phase emulsion structure of the pad secretion could prevent insects from slipping [99]. The hydrophobic droplets dispersed in a watery continuous phase could impart viscous and non-Newtonian (shear thinning) properties to the secretion for maximizing dynamic wet adhesion. Simple wet adhesion models, considering the contribution of the capillary and viscous forces, are often used to explain insect adhesion. However, for a more accurate representation, models should be expanded

to include the contribution of both the pad mechanical properties and viscous properties of the liquid adhesive. One recent study shows that the elastic deformation of the adhesive pad likely dominates the mechanical response when the adhesive secretions of animal are confined between elastic solids [33], and the authors utilize a fracture mechanics approach to estimate the adhesive mechanism of insects with the smooth adhesive pad.

3.1.3 Echinate Structure

Echinate structures normally have a limited contact area on hard and smooth surfaces because the adhesive force relies on the interaction between a few contacting tips of spines and a hard surface [100]. However, when the substrate is a soft or a fibrillar/hairy surface, the spiny structures can create unexpectedly strong adhesion by penetrating the surface and/or creating mechanical interlocking [18]. Adhesion associated with penetration is much harder to explain with simple models of dry or wet adhesion, and fibrillar or smooth structures, so the details of the comprehensive mechanism still remain elusive.

Strong and tailored adhesion based on surface topography has a significant role in the active locomotion of animals, but it is also essential for the passive transport of plant pollens and seeds. Pollens are one example to show how the size and shape of nanoscale features can be utilized for adhering selectively to specific surfaces [19]. The surface of some flowering pollens consists of a structured exine, which interacts with pollinators and stigmas, and the exine is often covered by a viscous liquid coating, pollenkitt [101]. It is known that the adhesion of pollens to the stigma of the same species or family is often much stronger than to another species, suggesting a physically-specific adhesion [102, 103]. For instance, the adhesive force magnitude of pollens from Asteraceae (sunflower) and Oleaceae (olive) families on stigma from Asteraceae was directly measured by AFM. The results showed that the echinate (spiny) structure of sunflower pollens strongly affects the adhesive mechanism of the pollen–stigma interaction on Asteraceae but not Oleaceae [18].

The sunflower pollen particle (Fig. 8a) has a spherical core body (30 ± 4 μm in diameter) with 1.5–2 μm-long spines, as shown in Fig. 8d. Structurally-derived load-dependent adhesion was attributed to the interlocking between the conical spines on the pollen surface and the stigma's receptive papillae (Fig. 8a). Previously, it was reported that the main contribution of the selective pollen–stigma interaction was dry adhesion (vdW interaction), as no significant difference of force magnitude was observed when the viscous liquid (pollenkitt) on the pollen surfaces was washed by organic solvents [19]. However, it is hard to generalize this observation because different species of pollen carry different amounts of pollenkitt. The contribution of the wet adhesive force attributed to pollenkitt seems to be comparable to the contribution of dry adhesion when pollens are coated with a sufficient amount (more than 30 wt% of innate pollens) of pollenkitt [76]. Moreover, it was shown that adhesion between unpurified pollens (coated

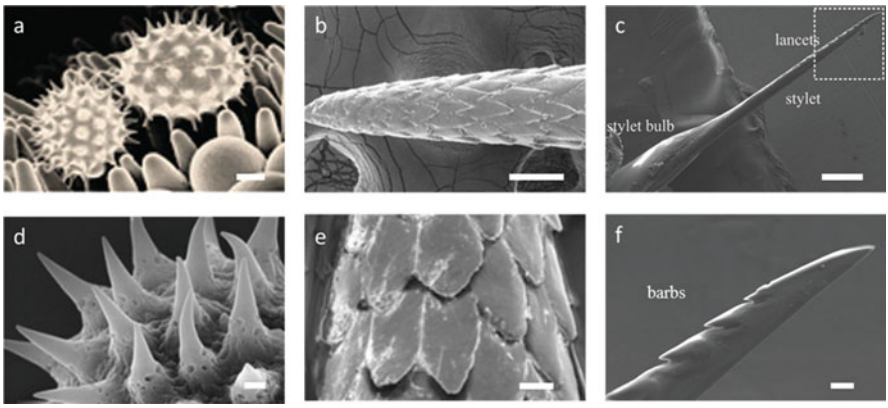

Fig. 8 Scanning electron microscopy (SEM) images of sunflower (*Helianthus annuus*) pollen on the stigma (**a**) and spiny structures on the sunflower pollen (**d**). (Reproduced from Lin et al. [18] with permission from Royal Society of Chemistry.) SEM images of the tip of a North American porcupine quill (**b**) and microstructures (barbs) on the tip (**e**). (Reproduced with permission from Cho et al. [104].) SEM images of stinger of honeybee (*Apis cerana cerana*) (**c**) and the tip of stinger and barbs near tip (**f**). (Reproduced with permission from Ling et al. [105].) *Scale bars* = 5 μm (**a**), 100 μm (**b**), 200 μm (**c**), 500 nm (**d**), 20 μm (**e**), and 10 μm (**f**)

with pollenkitt) and stigma-mimetic polymer surfaces had more than doubled adhesive magnitude when compared to purified pollens. In addition, the selective interaction between pollens and stigmas from the same botanical families was also observed when liquid pollenkitt wetted the surfaces [18].

In nature, many animals and plants utilize spiny features to protect themselves from natural predators, and these features can produce adhesion by penetration into tissue. North American porcupines utilize micro-structured barbs (Fig. 8b, e) on the tip of their specialized quills [104]. The conical shape of the tip is covered by a layer of backward-facing micro-structured barbs, which are 100–120 μm long and 35–45 μm wide (Fig. 8e). Compared with barbless quills, structured quills required 54% less loading force to penetrate into tissue, but required about four times larger pull-out force to be detached from the tissue surface. This suggests that the high-stress concentration near the barbs reduces the required force to deform the tissue around the tip of the quill, and the enhanced adhesion is attributed to the mechanical interlocking between barbs and tissue [104]. Micro-structured barbs (Fig. 8c, f) are also observed from the stingers of honeybees and paper wasps [106]. Different shapes of barbs are observed from those two animals, and the shape and size of the barbs strongly affect the penetration, extraction and the repeatable usage of their stingers. Similar mechanical interlocking adhesion on tissue surfaces is also observed in spiny-headed worms, such as *Pomphorhynchus laevis* [107]. This endoparasitic worm utilizes a barbed proboscis, which is swollen after embedding into the soft tissue of its host, to create strong adhesion.

3.2 *Bioadhesion on Rough Surfaces*

It is well-known that surface roughness reduces adhesion between relatively dry surfaces because the actual contact area is strongly affected by the surface topography [51, 52]. To achieve close contact on a rough surface, two different types of adhesive pads, which are smooth and fibrillar in structure, are utilized by animals, as discussed in Sect. 3.1. However, the roughness adaptability efficiency of adhesive pads can differ significantly. For example, when the scale of the surface asperity of a rough surface is smaller than the dimensions of the spatulae of the fibrillar system, only partial contact formation between the spatula and the surface is achieved [77]. Additional energy (loading energy) is required to achieve a close contact between a smooth pad and rough surface because the deformation of the pad surface is needed, and the required energy becomes maximized at an intermediate level of surface roughness [108]. Therefore, the attachment ability of adhesive pads is strongly dependent on surface roughness as shown in Fig. 9, and attachment ability is dramatically reduced near a particular scale of roughness, called the critical roughness [77, 109, 110].

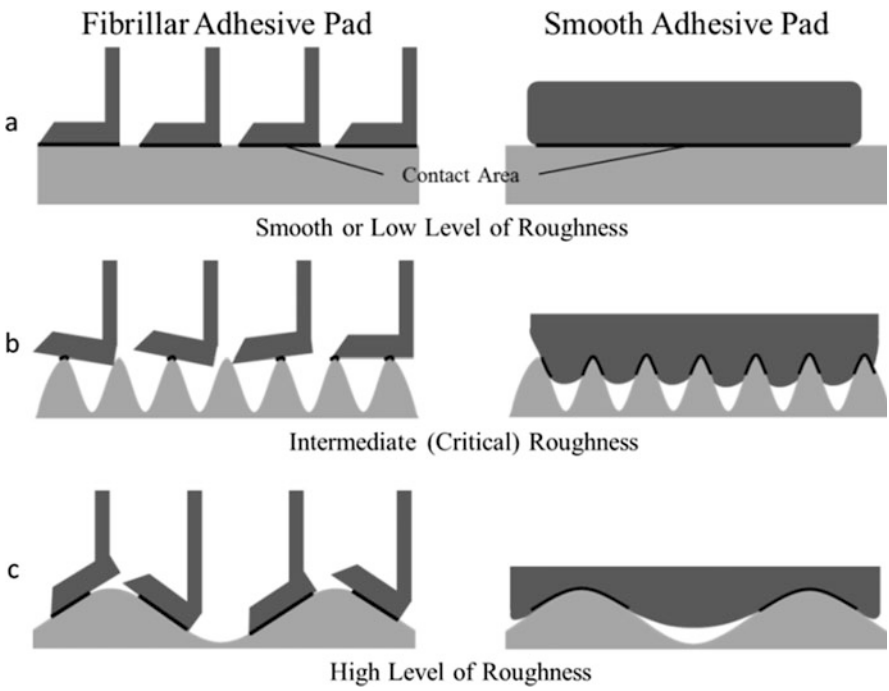

Fig. 9 Diagram explaining the influence of surface roughness on the roughness adaptability of fibrillar and smooth adhesive systems. (**a**) Large contact area on a smooth surface. (**b**) Partial contact formation on surface with critical roughness. (**c**) Roughness adaptability on a surface with a high roughness

When fibrillar adhesive structure is utilized by animals such as geckos, spiders, flies, and beetles to generate strong adhesion on rough surfaces, the dimension of the fibrils is a crucial factor for creating surface adaptability. For example, the length of adhesive hairs should be sufficient to deform around large asperities and thin enough to accommodate fine-scale surface roughness [111]. In a previous study, the attachment ability of a single hair (seta) was investigated to study the influence of surface roughness on gecko adhesion [77]. The pull-off force of a single hair was measured as a function of the surface root mean square (RMS) roughness from 20 to 1,100 nm. The relationship between adhesion and RMS roughness resembled an inverted parabola, with a distinctive minimum between 100 and 300 nm RMS roughness. The diameter of a single spatula of the gecko's adhesive pad is about 200 nm, and the surface adaptability of both a single spatula and the gecko itself was not efficient when surface roughness was close to the spatular dimension.

In experiments on the adhesion of other animals utilizing the fibrillar system, such as flies [112], beetles [111], and spiders [109], the critical roughness was investigated for substrates with an asperity size in the range 0.3–1 μm. According to previous studies, the spatula dimensions of geckos (0.2 μm) and spiders (0.7 μm) are smaller than those of flies (1.8 μm) and beetles (6 μm). As shown in Fig. 10a, there is a greater reduction of adhesion forces when substrate roughness is below the critical roughness for animals utilizing larger contact-forming elements [109]. Conversely, the fibrillar systems with smaller spatulae create relatively stronger adhesion than the larger spatulae on a surface with roughness below the critical value.

The geometrical scale of surface morphology in nature varies by seven to nine orders of magnitude, and the attachment organs of many animals, such as nanoscale

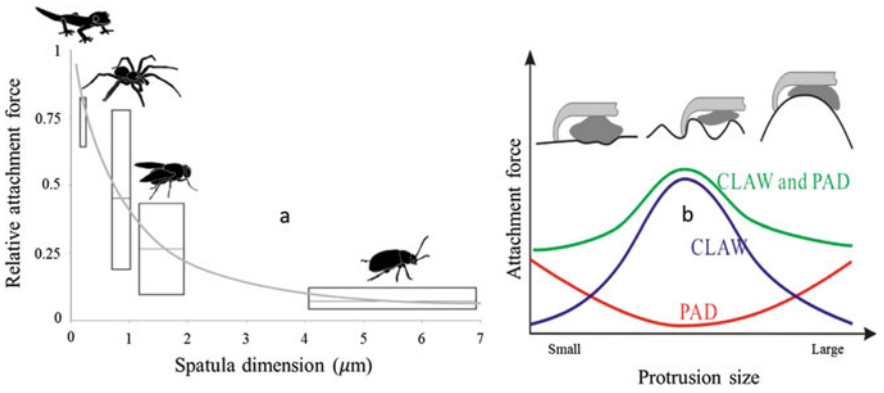

Fig. 10 (**a**) Comparison of force reduction on the intermediate level of rough surface (surface asperity size, 0.3 μm) as a function of spatula dimension. The attachment forces are normalized to the measured force on smooth surface. (Reproduced with permission from Wolff et al. [109].) (**b**) Diagram explaining the contribution of adhesive pad and claw on the wide range of protrusion size. (Reproduced with permission from Song et al. [108])

spatulae and macroscopic claws, have been optimized to generate adhesion on a wide range of surface asperities [108]. Many insects utilize rigid claws to create strong mechanical interlocking on microscopic surface irregularities when they stand or move on rough surfaces [108, 110, 111]. They are able to take advantage of the surface irregularities and use them as anchorage when the surface roughness is larger or compatible to the size of their claw tips.

In a previous study, the detachment forces of dock beetles, *Gastrophysa viridula* (with fibrillar adhesive pads and intact claws) and the same beetles without claws (adhesive pads only) were investigated as a function of surface roughness [111]. On smooth substrates (roughness, 0.01–1 μm), clawless beetles produced nearly the same magnitude of adhesion as intact beetles, but intact beetles produced a significantly larger force on larger scale roughness (12–30 μm) than clawless beetles. Theoretically, the maximum attachment ability of the beetle's fibrillar pad should be achieved on the smoothest substrates (roughness = 0.01 μm), but the intact beetles generated much stronger adhesion on the substrates with larger scale roughness (>5 μm). This force enhancement indicates that claws become more efficient at adhesion than pads when the surface roughness is close to the dimension of the claw tip, a diameter of 2.6 μm. The attachment ability of locusts (smooth adhesive pads with claws) also showed a similar response to surface roughness changes [110]. The measured attachment ability of the locust (critical roughness 1 μm) on rough surfaces (roughness > 5 μm) was stronger than on smooth surfaces, indicating that the contribution of the claws became significant when the surface roughness was greater than 5 μm. However, a recent study showed that the attachment ability of claws decreases when the surface asperity is much larger than the size of claw tips (Fig. 10b) [108]. Thus, the synergistic effect between claws and adhesive pads may generate stronger adhesion on various surface roughnesses than the sum of claws and adhesive pads alone.

4 Anti-adhesive Surfaces

In this section we discuss how substrate surface topography of substrates can be manipulated to reduce bioadhesion. Several strategies for creating anti-adhesive or slippery surfaces via surface topography have been proposed: (1) reducing the real contact area by controlling surface topography [20, 110, 111, 113], (2) contamination of the adhesive pad by fracturing of highly fragile surfaces [114–117], (3) absorbing the adhesive secretions into structured substrates [89], and (4) infusing a lubricating liquid that becomes locked in place by special structures [36]. Strategies (1)–(3) are examples of reduced adhesion (defined as energy required to separate two surfaces by pulling normal to one another) and (4) is an example of a slippery surface (low shear resistance or low friction lateral to the surface) that still retains adhesive characteristics (normal forces).

It is well-known that surface topography strongly affects the real contact area between surfaces. Even though animals have adapted features to adhere to

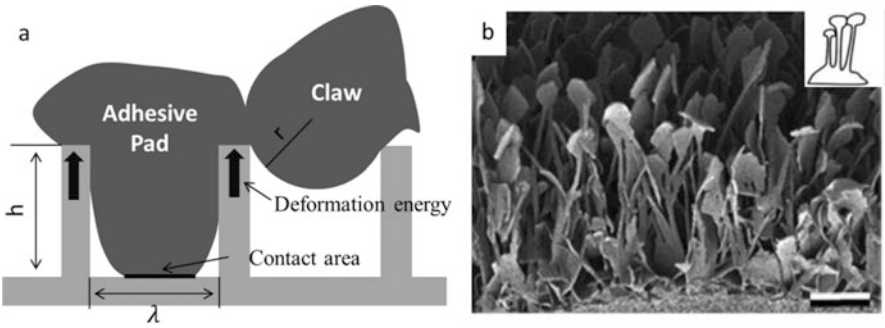

Fig. 11 (**a**) Diagram explaining the adhesive model of an adhesive pad and a claw with mathematical simplicity as a flat surface with walls of negligible thickness and height (h) which are spaced at a distance (λ). (**b**) Cryo-SEM microscopy image of the slippery zone wax coverage of *N. alata* (upper and lower wax layers connected by thin stalk). *Scale bar* = 1 μm. (Reproduced with permission from Gorb et al. [117])

structured surfaces, there is an opportunity to minimize adhesion by decreasing the feature size to achieve roughness below a critical value, a concept described in Sect. 3.2 [77, 109, 110]. In a previous study, the adhesion and deformation energy of adhesive pads and claws (with tip radius r) on a structured surface were modeled, as shown in Fig. 11a [20]. Interestingly, the results showed a finite range of wall sizes (h) and spacings (λ) where the required deformation energy to achieve a close contact is comparable to the adhesion energy. This indicates that, in theory, low adhesion surfaces, to which it is difficult for insect pads and claws to remain attached, can be designed by controlling surface topography. However, animals have different sizes and shapes of adhesive pads and claws, and the critical roughness required for each adhesive system varies according to this structural diversity. For example, the critical roughness of the locust (arithmetical mean roughness R_a = 1.0–2.0 μm) is one or two orders of magnitude higher than for the beetle (R_a = 0.01–0.13 μm) [110, 111]. Recent studies show that the design of hierarchical surface roughness consisting of small scale critical roughness (R_a = 0.01–0.13 μm) distributed on features with larger scale critical roughness (R_a = 1.0–2.0 μm) can be used to create anti-adhesive surfaces for both locusts and beetles [113, 118]. This idea has been extended to the development of icephobic [23, 119, 120] and insect mitigation coatings [121, 122]. It has been proposed that ice adhesion on multi-textured surfaces may be reduced because of trapped air bubbles as well as delayed ice nucleation [122]. The regular raised riblets of biofouling-resistant shark skin have led to bioinspired pillar/ridge [123] and 'wrinkled' [24] surface structures that resist adherence of biofouling organisms. In addition to shark skin, the microtextured surfaces of mussels and crabs are known to resist adhesion of biofouling organisms, a topic that has been reviewed extensively [124–126]. Based on the aforementioned bioadhesion studies, future research in optimizing surface topography is warranted.

Insects utilize adhesive pads and claws to generate strong adhesion, and the contribution of the claws of insects can be eliminated by adding submicron surface morphology, as the dimension of many of insect claws is on the micron scale or larger. However, it is challenging to design a universal surface roughness to reduce the functionality of the insects' adhesive pads because, as previously mentioned, each adhesive pad has a different critical roughness. A solution to overcome this challenge, suggested by Gorb et al., is to reduce insect adhesion by 'structural contamination' [115]. If the surface asperities of a substrate can be designed to break off under the loading of the animal body mass, the pieces may remain adhered to the insect adhesive pad and undermine the effectiveness of those features on enhancing adhesion. This strategy is inspired by the surface structure of the anti-adhesive zone in a carnivorous plant (*Nepenthes*). In previous studies of insect locomotion on the slippery zone, insects with smooth or fibrillar adhesive pads were unable to move, or moved only very slowly, because of reduced contact area caused by surface contamination attributed to the bilayer wax structure [114, 116]. The surface of the anti-adhesion zone is covered with upper and lower wax layers, and the platelet shape of the upper layer is connected to the lower layer with thin and long stalks, as shown in Fig. 11b [117]. There are three expected topographical effects that could lead to the reduction of insect adhesion: (1) the perpendicular orientation of the upper platelets reduces the contact area of the insect [20], (2) the long and thin stalk can break off during locomotion [127], contaminating the adhesive pads [114], and (3) the mechanical interlocking function of the claw cannot function because of the platelet's small dimension and their fragile and brittle nature [116]. In a recent study, the bilayer wax surfaces showed much better anti-adhesive functionality than substrates with roughness similar to the single lower wax layer [116]. This result indicates that the combination of the sacrificial structural features, mimicking the contaminated pads, and critical roughness strategies can improve anti-adhesive functionality.

Insects utilize a liquid secretion to increase the effective contact area on a rough surface. A loss of adhesive function of the insect foot pad was observed when the liquid secretion on the pad was washed with organic solvent [128]. Physical models and previous experiments also suggested that excessive volumes of the adhesive secretion reduce attachment ability because of hydrodynamic lubrication [59, 88]. These studies indicated that the attachment ability of liquid-based bioadhesive systems can be reduced or eliminated if the structure of substrates can increase or reduce the volume of the liquid secretion between the pad and substrate. For example, the adhesion of ladybird beetles on a nanoporous substrate was measured [89], and a significant drop of the attachment ability was observed on the nanoporous substrate compared to the adhesion on a smooth substrate. The authors claimed that the beetle secretion was absorbed by the porous substrate, causing reduced adhesion. To work effectively, the absorption rate of the structure must be faster than the production and delivery rate of the liquid secretion. Alternatively, to increase the liquid volume between the adhesive pad and rough substrate, a surface coated with a lubricating liquid was suggested [129–131]. However, the liquid coating on the surface might easily flow away by low shear forces or

even gravitational force. Recently, inspired by the continuously-wetted textured ridges of the peristome of *N. alata*, synthetic liquid-infused porous surfaces (SLIPS) were developed to create a stable lubricant film and impart slipperiness to interfaces [22, 36]. Key factors in retaining the infused lubrication fluid were the nanometer- and micrometer-scale porous and textured structures of the substrate. The attachment ability of the carpenter ant was tested on the SLIPS wall (perpendicular to gravity), which showed reliable low-friction functionality [36], causing the insects to slide and fail to attach. SLIPS structures have also been shown to impart icephobic characteristics to interfaces [22]. Interestingly, SLIPS have been shown to have exceptional biofouling resistant properties as well [132].

5 Conclusion

In this chapter we have summarized the physical principles of roughness and surface feature effects on adhesion, starting with simple geometries (such as spherical and planar surfaces) and expanding to consider complex surface morphologies. Both dry and wet adhesive mechanisms have been considered. Although there are no universal, simple models that capture all adhesive mechanisms, surface topography has been recognized as the most critical factor in determining adhesive properties. The evolutionarily-adapted surface structures of animals and plants show how surface topography can be utilized to create functionalized adhesive properties. The bioadhesive mechanisms of many of these structured surfaces have been investigated in order to mimic their adhesive functionality. Based on these investigations, diverse applications, such as surfaces for water-repellency, oil-water separation, and water purification, as well as anti-icing, anti-corrosion, and anti-bacterial surfaces, have been proposed or developed [23, 36, 133–136]. Further studies of structural effects may suggest designs for anti-adhesive and anti-icing surfaces for eliminating the detrimental impacts of aerodynamic residues, such as insects and ice, on transportation industries and other contamination-mitigating surfaces for extreme environments.

References

1. Shirtcliffe NJ, McHale G, Atherton S, Newton MI (2010) An introduction to superhydrophobicity. Adv Colloid Interf Sci 161:124–138. https://doi.org/10.1016/j.cis.2009.11.001
2. Lv J, Song Y, Jiang L, Wang J (2014) Bioinspired strategies for anti-icing. ACS Nano 8:3152–3169. https://doi.org/10.1021/nn406522n
3. Lee A, Moon MW, Lim H et al (2012) Water harvest via dewing. Langmuir 28:10183–10191. https://doi.org/10.1021/la3013987
4. Park K-C, Kim P, Grinthal A et al (2016) Condensation on slippery asymmetric bumps. Nature 531:78–82. https://doi.org/10.1038/nature16956

5. Gu ZZ, Uetsuka H, Takahashi K et al (2003) Structural color and the lotus effect. Angew Chem Int Ed 42:894–897. https://doi.org/10.1002/anie.200390235
6. Bechert DW, Bruse M, Hage W et al (1997) Experiments on drag-reducing surfaces and their optimization with an adjustable geometry. J Fluid Mech 338:59–87. https://doi.org/10.1017/S0022112096004673
7. Geim AK, Dubonos SV, Grigorieva IV et al (2003) Microfabricated adhesive mimicking gecko foot-hair. Nat Mater 2:461–463. https://doi.org/10.1038/nmat917
8. Hao P, Yao Z, Zhang X (2011) Study of dynamic hydrophobicity of micro-structured hydrophobic surfaces and lotus leaves. Sci China Phys Mech Astron 54:675–682. https://doi.org/10.1007/s11433-011-4269-1
9. Barthlott W, Neinhuis C (1997) Purity of the sacred lotus, or escape from contamination in biological surfaces. Planta 202:1–8. https://doi.org/10.1007/s004250050096
10. Parker AR, Lawrence CR (2001) Water capture by a desert beetle. Nature 414:33–34. https://doi.org/10.1038/35102108
11. Parker AR, Townley HE (2007) Biomimetics of photonic nanostructures. Nat Nanotechnol 2:347–353. https://doi.org/10.1038/nnano.2007.152
12. Luo Y, Liu Y, Anderson J et al (2015) Improvement of water-repellent and hydrodynamic drag reduction properties on bioinspired surface and exploring sharkskin effect mechanism. Appl Phys A Mater Sci Process 120:369–377. https://doi.org/10.1007/s00339-015-9198-9
13. Autumn K, Liang YA, Hsieh ST et al (2000) Adhesive force of a single gecko foot-hair. Nature 405:681–685
14. Federle W, Barnes WJP, Baumgartner W et al (2006) Wet but not slippery: boundary friction in tree frog adhesive toe pads. J R Soc Interface 3:689–697. https://doi.org/10.1098/rsif.2006.0135
15. Varenberg M, Pugno NM, Gorb SN (2010) Spatulate structures in biological fibrillar adhesion. Soft Matter 6:3269. https://doi.org/10.1039/c003207g
16. Spolenak R, Gorb S, Gao H, Arzt E (2005) Effects of contact shape on the scaling of biological attachments. Proc R Soc A Math Phys Eng Sci 461:305–319. https://doi.org/10.1098/rspa.2004.1326
17. Dirks JH, Li M, Kabla A, Federle W (2012) In vivo dynamics of the internal fibrous structure in smooth adhesive pads of insects. Acta Biomater 8:2730–2736. https://doi.org/10.1016/j.actbio.2012.04.008
18. Lin H, Qu Z, Meredith JC (2016) Pressure sensitive microparticle adhesion through biomimicry of the pollen-stigma interaction. Soft Matter 12:2965–2975. https://doi.org/10.1039/C5SM02845K
19. Edlund AF, Swanson R, Preuss D (2004) Pollen and stigma structure and function: the role of diversity in pollination. Plant Cell 16:S84–S97. https://doi.org/10.1105/tpc.015800
20. Scholz I, Bückins M, Dolge L et al (2010) Slippery surfaces of pitcher plants: nepenthes wax crystals minimize insect attachment via microscopic surface roughness. J Exp Biol 213:1115–1125. https://doi.org/10.1242/jeb.035618
21. Bauer U, Federle W (2009) The insect-trapping rim of nepenthes pitchers: surface structure and function. Plant Signal Behav 4:1019–1023. https://doi.org/10.4161/psb.4.11.9664
22. Kim P, Wong TS, Alvarenga J et al (2012) Liquid-infused nanostructured surfaces with extreme anti-ice and anti-frost performance. ACS Nano 6:6569–6577. https://doi.org/10.1021/nn302310q
23. Kreder MJ, Alvarenga J, Kim P, Aizenberg J (2016) Design of anti-icing surfaces: smooth, textured or slippery? Nat Rev Mater 1:15003. https://doi.org/10.1038/natrevmats.2015.3
24. Efimenko K, Finlay J, Callow ME et al (2009) Development and testing of hierarchically wrinkled coatings for marine antifouling. ACS Appl Mater Interfaces 1:1031–1040. https://doi.org/10.1021/am9000562
25. Hamaker HC (1937) The London—van der Waals attraction between spherical particles. Physica 4:1058–1072

26. Butt H-J, Kappl M (2009) Normal capillary forces. Adv Colloid Interf Sci 146:48–60. https://doi.org/10.1016/j.cis.2008.10.002
27. Mehrotra VP, Sastry KVS (1980) Pendular bond strength between unequal-sized spherical particles. Powder Technol 25:203–214. https://doi.org/10.1016/0032-5910(80)87031-8
28. Gu Y, Li D (1999) The van der Waals interaction between a spherical particle and a cylinder. J Colloid Interface Sci 217:60–69. https://doi.org/10.1006/jcis.1999.6349
29. Hartmann U (1991) Van der Waals interactions between sharp probes and flat sample surfaces. Phys Rev B 43:2404–2407. https://doi.org/10.1103/PhysRevB.43.2404
30. Tselishchev YG, Val'tsifer VA (2003) Influence of the type of contact between particles joined by a liquid bridge on the capillary cohesive forces. Colloid J 65:385–389. https://doi.org/10.1023/A:1024275327145
31. Tadmor R (2001) The London-van der Waals interaction energy between objects of various geometries. J Phys Condens Matter 13:L195–L202. https://doi.org/10.1088/0953-8984/13/9/101
32. Majumder A, Sharma A, Ghatak A (2010) Bioinspired adhesion and adhesives: controlling adhesion by micro-nano structuring of soft surfaces. In: Chakraborty S (ed) Microfluid. Microfabr. Springer, New York, pp 283–307. https://doi.org/10.1007/978-1-4419-1543-6_7
33. Labonte D, Federle W (2015) Rate-dependence of "wet" biological adhesives and the function of the pad secretion in insects. Soft Matter 11:8661–8673. https://doi.org/10.1039/C5SM01496D
34. Jagota A, Hui CY (2011) Adhesion, friction, and compliance of biomimetic and bioinspired structured interfaces. Mater Sci Eng R Rep 72:253–292. https://doi.org/10.1016/j.mser.2011.08.001
35. Wohl CJ, Smith JG, Palmieri FL, Connell JW (2017) The physics of insect impact and residue expansion. Adv Polym Sci (in press)
36. Wong T-S, Kang SH, Tang SKY et al (2011) Bioinspired self-repairing slippery surfaces with pressure-stable omniphobicity. Nature 477:443–447. https://doi.org/10.1038/nature10447
37. Gorb SN (2008) Biological attachment devices: exploring nature's diversity for biomimetics. Philos Transact A Math Phys Eng Sci 366:1557–1574. https://doi.org/10.1098/rsta.2007.2172
38. Gorb SN (2011) Biological fibrillar adhesives: functional principles and biomimetic applications. In: Handb Adhes Technol, pp 1409–1436. https://doi.org/10.1007/978-3-642-01169-6_54
39. Derks D, Lindner A, Creton C, Bonn D (2003) Cohesive failure of thin layers of soft model adhesives under tension. J Appl Phys 93:1557–1566. https://doi.org/10.1063/1.1533095
40. Croll S (2002) DLVO theory applied to TiO2 pigments and other materials in latex paints. Prog Org Coat 44:131–146. https://doi.org/10.1016/S0300-9440(01)00261-2
41. Lin L (2003) Mechanisms of pigment dispersion. Pigm Resin Technol 32:78–88. https://doi.org/10.1108/03699420310464784
42. Leite FL, Bueno CC, Da Róz AL et al (2012) Theoretical models for surface forces and adhesion and their measurement using atomic force microscopy. Int J Mol Sci 13(10):12773–12856. https://doi.org/10.3390/ijms131012773
43. Israelachvili JN (2010) Intermolecular and surface forces, 3rd edn. Academic Press, Cambridge, p 710. https://doi.org/10.1016/B978-0-12-375182-9.10025-9
44. Hertz H (1896) Miscellaneous papers. Macmillan, London
45. Johnson KL, Kendall K, Roberts AD (1971) Surface energy and the contact of elastic solids. Proc R Soc A Math Phys Eng Sci 324:301–313. https://doi.org/10.1098/rspa.1971.0141
46. Grierson DS, Flater EE, Carpick RW (2005) Accounting for the JKR-DMT transition in adhesion and friction measurements with atomic force microscopy. J Adhes Sci Technol 19:291–311. https://doi.org/10.1163/1568561054352685
47. Kamperman M, Kroner E, Del Campo A et al (2010) Functional adhesive surfaces with "Gecko" effect: the concept of contact splitting. Adv Eng Mater 12:335–348. https://doi.org/10.1002/adem.201000104

48. Derjaguin BV, Muller VM, Toporov YP (1975) Effect of contact deformations on the adhesion of particles. J Colloid Interface Sci 53:314–326. https://doi.org/10.1016/0021-9797(75)90018-1
49. Götzinger M, Peukert W (2004) Particle adhesion force distributions on rough surfaces. Langmuir 20:5298–5303. https://doi.org/10.1021/la049914f
50. Rabinovich YI, Adler JJ, Ata A et al (2000) Adhesion between nanoscale rough surfaces. J Colloid Interface Sci 232:10–16. https://doi.org/10.1006/jcis.2000.7167
51. Fuller KNG, Tabor D (1975) The effect of surface roughness on the adhesion of elastic solids. Proc R Soc A Math Phys Eng Sci 345:327–342. https://doi.org/10.1098/rspa.1975.0138
52. Persson BNJ, Tosatti E (2001) The effect of surface roughness on the adhesion of elastic solids. J Chem Phys 115:5597–5610. https://doi.org/10.1063/1.1398300
53. Rumpf H (1974) Die Wissenschaft des agglomerierens. Chem Ing Tech 46:1–11. https://doi.org/10.1002/cite.330460102
54. Gao H, Yao H (2004) Shape insensitive optimal adhesion of nanoscale fibrillar structures. Proc Natl Acad Sci U S A 101:7851–7856. https://doi.org/10.1073/pnas.0400757101
55. Eichenlaub S, Kumar G, Beaudoin S (2006) A modeling approach to describe the adhesion of rough, asymmetric particles to surfaces. J Colloid Interface Sci 299:656–664. https://doi.org/10.1016/j.jcis.2006.03.010
56. Prokopovich P, Starov V (2011) Adhesion models: from single to multiple asperity contacts. Adv Colloid Interf Sci 168:210–222. https://doi.org/10.1016/j.cis.2011.03.004
57. Yu J, Chary S, Das S et al (2012) Friction and adhesion of gecko-inspired PDMS flaps on rough surfaces. Langmuir 28:11527–11534. https://doi.org/10.1021/la301783q
58. Cai S, Bhushan B (2007) Meniscus and viscous forces during normal separation of liquid-mediated contacts. Nanotechnology 18:465704. https://doi.org/10.1088/0957-4484/18/46/465704
59. Dirks JH, Federle W (2011) Fluid-based adhesion in insects – principles and challenges. Soft Matter 7:11047. https://doi.org/10.1039/c1sm06269g
60. Dirks JH (2014) Physical principles of fluid-mediated insect attachment-shouldn't insects slip? Beilstein J Nanotechnol 5:1160–1166. https://doi.org/10.3762/bjnano.5.127
61. Orr FM, Scriven LE, Rivas AP (1975) Pendular rings between solids: meniscus properties and capillary force. J Fluid Mech 67:723. https://doi.org/10.1017/S0022112075000572
62. Matthewson MJ (1988) Adhesion of spheres by thin liquid films. Philos Mag A 57:207–216. https://doi.org/10.1080/01418618808204510
63. Ata A, Rabinovich Y, Singh R (2002) Role of surface roughness in capillary adhesion. J Adhes Sci Technol 4243:37–41. https://doi.org/10.1163/156856102760067145
64. Willett CD, Adams MJ, Johnson SA, Seville JPK (2000) Capillary bridges between two spherical bodies. Langmuir 16:9396–9405. https://doi.org/10.1021/la000657y
65. Rabinovich YI, Esayanur MS, Moudgil BM (2005) Capillary forces between two spheres with a fixed volume liquid bridge: theory and experiment. Langmuir 21:10992–10997. https://doi.org/10.1021/la0517639
66. Bhushan B (2003) Adhesion and stiction: mechanisms, measurement techniques, and methods for reduction. J Vac Sci Technol B Microelectron Nanom Struct 21:2262. https://doi.org/10.1116/1.1627336
67. Lee T, Charrault E, Neto C (2014) Interfacial slip on rough, patterned and soft surfaces: a review of experiments and simulations. Adv Colloid Interf Sci 210:21–38. https://doi.org/10.1016/j.cis.2014.02.015
68. Mongruel A, Chastel T, Asmolov ES, Vinogradova OI (2013) Effective hydrodynamic boundary conditions for microtextured surfaces. Phys Rev E Stat Nonlinear Soft Matter Phys 87:1–4. https://doi.org/10.1103/PhysRevE.87.011002
69. Kunert C, Harting J, Vinogradova OI (2010) Random-roughness hydrodynamic boundary conditions. Phys Rev Lett 105:2–5. https://doi.org/10.1103/PhysRevLett.105.016001

70. Maali A, Pan Y, Bhushan B, Charlaix E (2012) Hydrodynamic drag-force measurement and slip length on microstructured surfaces. Phys Rev E Stat Nonlinear Soft Matter Phys 85:1–5. https://doi.org/10.1103/PhysRevE.85.066310
71. Vinogradova OI (1995) Drainage of a thin liquid film confined between hydrophobic surfaces. Langmuir 11:2213–2220. https://doi.org/10.1021/la00006a059
72. Pilkington GA, Gupta R, Fréchette J (2016) Scaling hydrodynamic boundary conditions of microstructured surfaces in the thin channel limit. Langmuir 32:2360–2368. https://doi.org/10.1021/acs.langmuir.5b04134
73. Nizkaya TV, Dubov AL, Mourran A, Vinogradova OI (2016) Probing effective slippage on superhydrophobic surfaces by atomic force microscopy. Soft Matter 12:6910–6917. https://doi.org/10.1039/C6SM01074A
74. Creton C, Gorb SN (2007) Sticky feet: from animals to materials. MRS Bull 32:466–472
75. Pacini E, Hesse M (2005) Pollenkitt - its composition, forms and functions. Flora Morphol Distrib Funct Ecol Plants 200:399–415. https://doi.org/10.1016/j.flora.2005.02.006
76. Lin H, Gomez I, Meredith JC (2013) Pollenkitt wetting mechanism enables species-specific tunable pollen adhesion. Langmuir 29:3012–3023
77. Huber G, Gorb SN, Hosoda N et al (2007) Influence of surface roughness on gecko adhesion. Acta Biomater 3:607–610. https://doi.org/10.1016/j.actbio.2007.01.007
78. Lake GJ, Thomas AG (1967) The strength of highly elastic materials. Proc R Soc A Math Phys Eng Sci 300:108–119. https://doi.org/10.1098/rspa.1967.0160
79. Arzt E, Gorb S, Spolenak R (2003) From micro to nano contacts in biological attachment devices. Proc Natl Acad Sci U S A 100:10603–10606. https://doi.org/10.1073/pnas.1534701100
80. Peattie AM, Full RJ (2007) Phylogenetic analysis of the scaling of wet and dry biological fibrillar adhesives. Proc Natl Acad Sci 104:18595–18600. https://doi.org/10.1073/pnas.0707591104
81. Labonte D, Clemente CJ, Dittrich A et al (2016) Extreme positive allometry of animal adhesive pads and the size limits of adhesion-based climbing. Proc Natl Acad Sci 113:201519459. https://doi.org/10.1073/pnas.1519459113
82. Autumn K, Sitti M, Liang YA et al (2002) Evidence for van der Waals adhesion in gecko setae. Proc Natl Acad Sci U S A 99:12252–12256. https://doi.org/10.1073/pnas.192252799
83. Bhushan B, Sayer RA (2007) Gecko feet: natural attachment systems for smart adhesion. In: Appl Scanning Probe Methods VII, pp 41–76. https://doi.org/10.1007/11785705
84. Gao H, Wang X, Yao H et al (2005) Mechanics of hierarchical adhesion structures of geckos. Mech Mater 37:275–285. https://doi.org/10.1016/j.mechmat.2004.03.008
85. Bullock JMR, Drechsler P, Federle W (2008) Comparison of smooth and hairy attachment pads in insects: friction, adhesion and mechanisms for direction-dependence. J Exp Biol 211:3333–3343. https://doi.org/10.1242/jeb.020941
86. Autumn K, Majidi C, Groff RE et al (2006) Effective elastic modulus of isolated gecko setal arrays. J Exp Biol 209:3558–3568. https://doi.org/10.1242/jeb.02469
87. Tian Y, Pesika N, Zeng H et al (2006) Adhesion and friction in gecko toe attachment and detachment. Proc Natl Acad Sci U S A 103:19320–19325. https://doi.org/10.1073/pnas.0608841103
88. Drechsler P, Federle W (2006) Biomechanics of smooth adhesive pads in insects: influence of tarsal secretion on attachment performance. J Comp Physiol A Neuroethol Sens Neural Behav Physiol 192:1213–1222. https://doi.org/10.1007/s00359-006-0150-5
89. Gorb EV, Hosoda N, Miksch C, Gorb SN (2010) Slippery pores: anti-adhesive effect of nanoporous substrates on the beetle attachment system. J R Soc Interface 7:1571–1579. https://doi.org/10.1098/rsif.2010.0081
90. De Souza EJ, Brinkmann M, Mohrdieck C, Arzt E (2008) Enhancement of capillary forces by multiple liquid bridges. Langmuir 24:8813–8820. https://doi.org/10.1021/la8005376
91. Su Y, Ji B, Huang Y, Hwang K (2007) Effects of contact shape on biological wet adhesion. J Mater Sci 42:8885–8893. https://doi.org/10.1007/s10853-007-1759-7

92. Gorb S, Varenberg M (2007) Mushroom-shaped geometry of contact elements in biological adhesive systems. J Adhes Sci Technol 21:1175–1183. https://doi.org/10.1163/156856107782328317
93. Barnes WJP (2007) Functional morphology and design constraints of smooth adhesive pads. MRS Bull 32:479–485. https://doi.org/10.1557/mrs2007.81
94. Barnes WJP, Goodwyn PJP, Nokhbatolfoghahai M, Gorb SN (2011) Elastic modulus of tree frog adhesive toe pads. J Comp Physiol A Neuroethol Sens Neural Behav Physiol 197:969–978. https://doi.org/10.1007/s00359-011-0658-1
95. Barnes WJP, Oines C, Smith JM (2006) Whole animal measurements of shear and adhesive forces in adult tree frogs: insights into underlying mechanisms of adhesion obtained from studying the effects of size and scale. J Comp Physiol A Neuroethol Sens Neural Behav Physiol 192:1179–1191. https://doi.org/10.1007/s00359-006-0146-1
96. Scholz I, Barnes WJP, Smith JM, Baumgartner W (2009) Ultrastructure and physical properties of an adhesive surface, the toe pad epithelium of the tree frog, Litoria Caerulea white. J Exp Biol 212:155–162. https://doi.org/10.1242/jeb.019232
97. Iturri J, Xue L, Kappl M et al (2015) Torrent frog-inspired adhesives: attachment to flooded surfaces. Adv Funct Mater 25:1499–1505. https://doi.org/10.1002/adfm.201403751
98. Endlein T, Barnes WJP, Samuel DS et al (2013) Sticking under wet conditions: the remarkable attachment abilities of the torrent frog, Staurois Guttatus. PLoS One 8(9):e73810. https://doi.org/10.1371/journal.pone.0073810
99. Dirks J-H, Clemente CJ, Federle W (2010) Insect tricks: two-phasic foot pad secretion prevents slipping. J R Soc Interface 7:587–593. https://doi.org/10.1098/rsif.2009.0308
100. Thio BJR, Lee JH, Meredith JC (2009) Characterization of ragweed pollen adhesion to polyamides and polystyrene using atomic force microscopy. Environ Sci Technol 43:4308–4313
101. Lin H, Lizarraga L, Bottomley LA, Meredith JC (2015) Effect of water absorption on pollen adhesion. J Colloid Interface Sci 442:133–139. https://doi.org/10.1016/j.jcis.2014.11.065
102. Zinkl GM, Zwiebel BI, Grier DG, Preuss D (1999) Pollen-stigma adhesion in Arabidopsis: a species-specific interaction mediated by lipophilic molecules in the pollen exine. Development 126:5431–5440
103. Luu DT, Passelègue E, Dumas C, Heizmann P (1998) Pollen-stigma capture is not species discriminant within the Brassicaceae Family. C R Acad Sci III 321:747–755. https://doi.org/10.1016/S0764-4469(98)80015-2
104. Cho WK, Ankrum JA, Guo D et al (2012) Microstructured barbs on the north American porcupine quill enable easy tissue penetration and difficult removal. Proc Natl Acad Sci U S A 109:21289–21294. https://doi.org/10.1073/pnas.1216441109
105. Ling J, Jiang L, Chen K et al (2016) Insertion and pull behavior of worker honeybee stinger. J Bionic Eng 13:303–311. https://doi.org/10.1016/S1672-6529(16)60303-7
106. Zhao Z-L, Zhao H-P, Ma G-J et al (2015) Structures, properties, and functions of the stings of honey bees and paper wasps: a comparative study. Biol Open 4:921–928. https://doi.org/10.1242/bio.012195
107. Yang SY, O'Cearbhaill ED, Sisk GC et al (2013) A bioinspired swellable microneedle adhesive for mechanical interlocking with tissue. Nat Commun 4:1702. https://doi.org/10.1038/ncomms2715
108. Song Y, Dai Z, Wang Z et al (2016) The synergy between the insect-inspired claws and adhesive pads increases the attachment ability on various rough surfaces. Sci Rep 6:26219. https://doi.org/10.1038/srep26219
109. Wolff JO, Gorb SN (2012) Surface roughness effects on attachment ability of the spider Philodromus Dispar (Araneae, Philodromidae). J Exp Biol 215:179–184. https://doi.org/10.1242/jeb.061507
110. Wang L, Johannesson CM, Zhou Q (2015) Effect of surface roughness on attachment ability of locust Locusta migratoria manilensis. Wear 332:694–701. https://doi.org/10.1016/j.wear.2015.02.036

111. Bullock JMR, Federle W (2011) The effect of surface roughness on claw and adhesive hair performance in the dock beetle Gastrophysa viridula. Insect Sci 18:298–304. https://doi.org/10.1111/j.1744-7917.2010.01369.x
112. Peressadko AG, Gorb SN (2004) Surface profile and friction force generated by insects. In: First Int Ind Conf Bionik 2004, pp 257–261
113. Prüm B, Florian Bohn H, Seidel R et al (2013) Plant surfaces with cuticular folds and their replicas: influence of microstructuring and surface chemistry on the attachment of a leaf beetle. Acta Biomater 9:6360–6368. https://doi.org/10.1016/j.actbio.2013.01.030
114. Gaume L, Perret P, Gorb E et al (2004) How do plant waxes cause flies to slide? Experimental tests of wax-based trapping mechanisms in three pitfall carnivorous plants. Arthropod Struct Dev 33:103–111. https://doi.org/10.1016/j.asd.2003.11.005
115. Gorb E, Haas K, Henrich A et al (2005) Composite structure of the crystalline epicuticular wax layer of the slippery zone in the pitchers of the carnivorous plant Nepenthes alata and its effect on insect attachment. J Exp Biol 208:4651–4662. https://doi.org/10.1242/jeb.01939
116. Gorb EV, Purtov J, Gorb SN (2014) Adhesion force measurements on the two wax layers of the waxy zone in Nepenthes alata pitchers. Sci Rep 4:5154. https://doi.org/10.1038/srep05154
117. Gorb EV, Baum MJ, Gorb SN (2013) Development and regeneration ability of the wax coverage in Nepenthes alata pitchers: a cryo-SEM approach. Sci Rep 3:3078. https://doi.org/10.1038/srep03078
118. Eichler-Volf A, Kovalev A, Wedeking T et al (2016) Bioinspired monolithic polymer microsphere arrays as generically anti-adhesive surfaces. Bioinspir Biomim 11:25002. https://doi.org/10.1088/1748-3190/11/2/025002
119. Varanasi KK, Deng T, Smith JD et al (2010) Frost formation and ice adhesion on superhydrophobic surfaces. Appl Phys Lett 97:234102. https://doi.org/10.1063/1.3524513
120. Schutzius TM, Jung S, Maitra T et al (2015) Physics of icing and rational design of surfaces with extraordinary icephobicity. Langmuir 31:4807–4821. https://doi.org/10.1021/la502586a
121. Wohl CJ, Smith JG, Penner RK et al (2013) Evaluation of commercially available materials to mitigate insect residue adhesion on wing leading edge surfaces. Prog Org Coat 76:42–50. https://doi.org/10.1016/j.porgcoat.2012.08.009
122. Krishnan KG, Milionis A, Loth E et al (2017) Influence of hydrophobic and superhydrophobic surfaces on reducing aerodynamic insect residues. Appl Surf Sci 392:723–731. https://doi.org/10.1016/j.apsusc.2016.09.096
123. Carman ML, Estes TG, Feinberg AW et al (2006) Engineered antifouling microtopographies - correlating wettability with cell attachment. Biofouling 22:11–21. https://doi.org/10.1080/08927010500484854
124. Genzer J, Efimenko K (2006) Recent developments in superhydrophobic surfaces and their relevance to marine fouling: a review. Biofouling 22:339–360. https://doi.org/10.1080/08927010600980223
125. Scardino AJ, de Nys R (2011) Mini review: biomimetic models and bioinspired surfaces for fouling control. Biofouling 27:73–86. https://doi.org/10.1080/08927014.2010.536837
126. Magin CM, Cooper SP, Brennan AB (2010) Non-toxic antifouling strategies. Mater Today 13:36–44. https://doi.org/10.1016/S1369-7021(10)70058-4
127. Borodich FM, Gorb EV, Gorb SN (2010) Fracture behaviour of plant epicuticular wax crystals and its role in preventing insect attachment: a theoretical approach. Appl Phys A Mater Sci Process 100:63–71. https://doi.org/10.1007/s00339-010-5794-x
128. Edwards JS, Tarkanian M (1970) The adhesive pads of Heteroptera: a re-examination. Proc R Entomol Soc Lond A Gen Entomol 45:1–5
129. Bauer U, Federle W, Seidel H et al (2015) How to catch more prey with less effective traps: explaining the evolution of temporarily inactive traps in carnivorous pitcher plants. Proc Biol Sci 282:20142675. https://doi.org/10.1098/rspb.2014.2675

130. Bauer U, Bohn HF, Federle W (2008) Harmless nectar source or deadly trap: nepenthes pitchers are activated by rain, condensation and nectar. Proc Biol Sci 275:259–265. https://doi.org/10.1098/rspb.2007.1402
131. Bohn HF, Federle W (2004) Insect aquaplaning: nepenthes pitcher plants capture prey with the peristome, a fully wettable water-lubricated anisotropic surface. Proc Natl Acad Sci U S A 101:14138–14143. https://doi.org/10.1073/pnas.0405885101
132. Epstein AK, Wong T-S, Belisle RA et al (2012) Liquid-infused structured surfaces with exceptional anti-biofouling performance. Proc Natl Acad Sci U S A 109:13182–13187. https://doi.org/10.1073/pnas.1201973109
133. Darmanin T, Guittard F (2013) Recent advances in the potential applications of bioinspired superhydrophobic materials. R Soc Chem 0:1–3. https://doi.org/10.1039/C4TA02071E
134. Sun X, Damle VG, Liu S, Rykaczewski K (2015) Bioinspired stimuli-responsive and antifreeze-secreting anti-icing coatings. Adv Mater Interfaces 2:25–27. https://doi.org/10.1002/admi.201400479
135. Bhushan B (2012) Bioinspired structured surfaces. Langmuir 28:1698–1714. https://doi.org/10.1021/la2043729
136. Ivanova EP, Hasan J, Webb HK et al (2013) Bactericidal activity of black silicon. Nat Commun 4:2838. https://doi.org/10.1038/ncomms3838